Materials Today Bio 16 (2022) 100354

Contents lists available at ScienceDirect

Materials Today Bio

journal homepage: www.journals.elsevier.com/materials-today-bio

An ultra-sensitive electrochemical biosensor using the Spike protein for capturing antibodies against SARS-CoV-2 in point-of-care

Ana R. Cardoso [a,b,c], João Frederico Alves [a], Manuela F. Frasco [a], Ana Margarida Piloto [b], Verónica Serrano [a], Daniela Mateus [a,d], Ana Isabel Sebastião [d], Ana Miguel Matos [e], Anália Carmo [f], Teresa Cruz [d], Elvira Fortunato [c], M. Goreti F. Sales [a,b,*]

[a] BioMark@UC/CEB - LABBELS, Faculty of Sciences and Technology, University of Coimbra, Coimbra, Portugal
[b] BioMark@ISEP/ CEB - LABBELS, School of Engineering, Polytechnic Institute of Porto, Porto, Portugal
[c] CENIMAT|i3N, Department of Materials Science, School of Science and Technology, NOVA University of Lisbon and CEMOP/UNINOVA, Campus de Caparica, 2829-516, Caparica, Portugal
[d] Center for Neuroscience and Cell Biology, Faculty of Pharmacy, University of Coimbra, Coimbra, Portugal
[e] Chemical Engineering Processes and Forest Products Research Center, Faculty of Pharmacy, University of Coimbra, Coimbra, Portugal
[f] Clinical Pathology Department, Centro Hospitalar e Universitário de Coimbra, Coimbra, Portugal

ARTICLE INFO

Keywords:
Electrochemical biosensor
Antibodies for SARS-CoV-2
SARS-CoV-2
Spike protein
Protective immunity
Point-of-care

ABSTRACT

This work presents an innovative ultra-sensitive biosensor having the Spike protein on carbon-based screen-printed electrodes (SPEs), for monitoring in point-of-care antibodies against SARS-CoV-2, a very important tool for epidemiological monitoring of COVID-19 infection and establishing vaccination schemes. In an innovative and simple approach, a highly conductive support is combined with the direct adsorption of Spike protein to enable an extensive antibody capture. The high conductivity was ensured by using carboxylated carbon nanotubes on the carbon electrode, by means of a simple and quick approach, which also increased the surface area. These were then modified with EDC/NHS chemistry to produce an amine layer and undergo Spike protein adsorption, to generate a stable layer capable of capturing the antibodies against SARS-CoV-2 in serum with great sensitivity. Electrochemical impedance spectroscopy was used to evaluate the analytical performance of this biosensor in serum. It displayed a linear response between 1.0 pg/mL and 10 ng/mL, with a detection limit of ~0.7 pg/mL. The analysis of human positive sera containing antibody in a wide range of concentrations yielded accurate data, correlating well with the reference method. It also offered the unique ability of discriminating antibody concentrations in sera below 2.3 μg/mL, the lowest value detected by the commercial method. In addition, a proof-of-concept study was performed by labelling anti-IgG antibodies with quantum dots to explore a new electrochemical readout based on the signal generated upon binding to the anti-S protein antibodies recognised on the surface of the biosensor. Overall, the alternative serologic assay presented is a promising tool for assessing protective immunity to SARS-CoV-2 and a potential guide for revaccination.

1. Introduction

In just two decades of the 21st century, numerous viral epidemics/pandemics have occurred that have been recognised by the World Health Organization. These include Severe Acute Respiratory Syndrome Coronavirus (SARS-CoV, 2003), Chikungunya (2005), Influenza A (H1N1) (2009), Middle East Respiratory Syndrome Coronavirus (MERS-CoV, 2012), Ebola (2014, 2019), and Zika (2015/2016) [1]. Such frequent outbreaks are evidence that future pandemics can be expected [2]. In this context, zoonotic viruses are considered the leading potential pathogens, for which there are neither effective vaccines nor drugs. The most compelling example is the recent outbreak of Severe Acute Respiratory Syndrome Coronavirus 2 (SARS-CoV-2), which triggered Coronavirus Disease 2019 (COVID -19) with devastating effects worldwide [3].

The highly contagious properties led to a rapid increase in the number of infected individuals. The high prevalence of asymptomatic individuals has also led to a high rate of transmission of the disease. Although there are no accurate quantitative data in the literature, reports suggest that

* Corresponding author. BioMark@UC/CEB - LABBELS, Faculty of Sciences and Technology, University of Coimbra, Coimbra, Portugal.
E-mail addresses: goreti.sales@eq.uc.pt, goreti.sales@gmail.com (M.G.F. Sales).

https://doi.org/10.1016/j.mtbio.2022.100354
Received 5 May 2022; Received in revised form 2 July 2022; Accepted 5 July 2022
Available online 9 July 2022

approximately 30% of the population exposed to the virus is asymptomatic and transmits the disease. In addition, the signs of COVID -19 are nonspecific and include respiratory symptoms, fever, cough, dyspnoea, and viral pneumonia that require biochemical testing for diagnosis. Although the inherent infectious properties of the virus cannot be altered, it is possible to improve the biochemical tests that are currently being conducted worldwide to stratify the population, monitor the level of immunity in the community, and conduct viral surveillance [4].

Separating those infected (who must remain in quarantine) from those who have an immunological response against the virus (antibodies) is essential for controlling pandemics and improving the global economic scenario. This will allow a portion of the population to return to their "normal" activities without risk. In addition, in order for currently available vaccines to be administered, it must be demonstrated that antibodies against SARS-CoV-2 have formed, and it must be known how they develop in individuals over time and how they subside over time. This is especially important at the community level, but difficult to implement at the global level [5].

Overall, monitoring of antibody levels is necessary to guide antiviral treatment, infection control, epidemiologic measures, and vaccination. Serologic testing is essential for evaluating the qualitative and quantitative results of immune responses and has proven to be a valuable tool since the onset of infection. These tests are important public health tools to limit the risk of exposure and unintentional spread of the virus. This could be critical to limit the global spread of the disease and allow for the establishment of checkpoints for people in transit, including airports. In addition, a global antibody test would also allow stratification of populations by no, weak, moderate, or strong immune response, which is particularly important for achieving our "normal" life [6,7].

Therefore, tools should be available to detect SARS-CoV-2 antibodies in the general population at different time points for each individual. Current methods include enzyme-linked immunosorbent assay (ELISA) tests, which are neither rapid enough to allow immediate action nor sensitive enough to detect early stages of viral infection and disease onset. They also require laboratory facilities and specific equipment and reagents. In addition, some of these reagents are expensive and not available to meet global needs [8,9].

Alternative rapid systems using biosensors have also been developed. These could be ideal modern tools as they have the potential to develop simple and inexpensive devices with low limits of detection for anti-SARS CoV-2 antibodies. Currently, lateral flow assays are the most popular biosensors for SARS CoV-2 serological assays because they have several advantages, such as ease of use and rapid response time. However, they have limited sensitivity and sensing capability compared to biosensors and are also more expensive [8]. In contrast, electrochemical biosensors can provide efficient, rapid, and accurate analysis, for which many papers have been published in the literature using this technology [10]. However, electrochemical biosensors also face some challenges that delay technology transfer to reach commercialization at the point-of-care [11].

Recent works on antibody detection can use renewable materials as substrates [12], optical techniques with special engineered antibodies [13] or plasmonic-based readout devices [14] and specially designed nanostructure arrays [15]. Overall, these works provide good analytical properties but require several steps for electrode assembly, which can be very complex and/or require specialised and expensive instrumentation. Therefore, a simple biosensor for serological monitoring of SARS-CoV-2 antibodies is still lacking in the literature, which is particularly important to allow scaling up to an industrial production and their global use.

The performance of an electrochemical biosensor depends on the characteristics of the electrode's interface and external conditions. Immobilization capacity, sensitivity, conductivity or specificity of the biosensor may be affected by the electrode's surface area and material composition [16,17]. Therefore, nanomaterials emerge as a promising resource to modify the electrode's interface to enhance its efficiency characteristics, improving the biosensor analytical performance. Carbon nanomaterials are particularly suitable for carbon electrodes and engineering their atomic properties allow for a variety of carbon allotropes that might answer to a diverse range of applications [18]. Carboxylated single-walled carbon nanotubes (SWCNTs), formed by a nanoscale graphene sheet folded around itself, are characterized by strong covalent bonding, high tensile strength, improved electron transfer, high surface area-to-weight ratio and porosity (important for protein immobilization) and good thermal stability (which may have a positive impact on the reproducibility of the sensor) [16,19,20].

Additionally, engineered nanoparticles may also be used as electrochemical labels. Cadmium telluride quantum dots (CdTe QDs) are colloidal semiconductor fluorescent nanoscale crystals that can be easily modified with biomolecules such as antibodies, generally improve the stability of the sensor as well as its photoelectric properties [21–23], and present good interaction with carbon nanotubes [24], making these nanoparticles an interesting electrochemical probe for our biosensor.

Thus, this article presents a sensitive electrochemical biosensor that, although assembled using an amazingly simple procedure, can detect small amounts of antibodies in human serum (and in much smaller amounts than conventional methods). The biosensor uses commercially available screen-printed electrodes (SPEs) with a carbon working electrode containing *p*-phenylenediamine and protein S. Analytical properties are evaluated, and the devices are tested in human serum and further validated using a commercial benchmark method restricted to laboratory facilities. Electrochemical detection is performed in two ways: with an iron redox probe or with anti-IgG labelled with QDs.

2. Experimental section

2.1. Reagents and solutions

All chemicals were of analytical grade and ultrapure Milli-Q water laboratory grade (conductivity <0.1 μS/cm) was used. Chemical reagents included potassium hexacyanoferrate III ($K_3[Fe(CN)_6]$) from Carlo Erba; potassium hexacyanoferrate II ($K_4[Fe(CN)_6]$) trihydrate from Panreac; carboxylated single-walled carbon nanotubes (SWCNT); *N*-ethyl-*N*'-(3-dimethylaminopropyl) carbodiimide hydrochloride (EDAC), *p*-phenylenediamine, phosphate buffered saline (PBS, 0.01 mol/L, pH 7.4), *N,N*-dimethylformamide (DMF) were purchased from Sigma-Aldrich; *N*-hydroxysuccinimide (NHS) was acquired from Merck; recombinant SARS-CoV-2 Spike protein, S1 subunit, Host Cell Receptor Binding Domain (RBD), rabbit anti-SARS-CoV-2 S protein antibody, and rabbit anti-SARS-CoV-2 nucleocapsid (N) protein antibody were obtained from RayBiotech.

2.2. Apparatus

Electrochemical measurements were performed using a PalmSens4 potentiostat/galvanostat controlled by PSTrace 5.8 software. Commercial carbon SPEs (C-SPEs) from Metrohm DropSens (DRP-110) were used. These contain a three-electrode system, including: (a) a carbon counter electrode, (b) a silver reference electrode, and (c) a 4 mm diameter carbon working electrode. The C-SPEs were connected to a PalmSens switch box that allows connection to the potentiostat.

2.3. Electrochemical measurements

Cyclic voltammetry (CV) was performed in the range of -0.3 to $+0.7$ V at a scan rate of 50 mV/s. Electrochemical impedance spectroscopy (EIS) was performed in open circuit with a sinusoidal potential perturbation with an amplitude of 0.01 V and 50 data points logarithmically distributed over a frequency range of 0.1–100000 Hz. The SWV data require a sampling potential of -0.3 to $+0.7$ V, with a frequency of 2 Hz and a step height of up to 2.5 mV.

For the EIS data, Nyquist plots were used to represent the spectra obtained, showing the frequency response of the electrolyte system and

plotting the imaginary component (Z″) of the impedance against its real component (Z′). The EIS data were fitted to the typical Randles equivalent circuit, typically employed in impedimetric biosensors, and being composed herein of solution resistance (Rs), double layer capacitance (C_{dl}), and charge transfer resistance (Rct) [25–28]. R_S is the resistance between the working and reference electrode. R_{CT} is the electron transfer resistance across the electrode-electrolyte interface. C_{dl} is the specific capacitance at the interface of the electrolyte and the electrode and is characterized by the non-faradaic charge that arises from the surface. Analysing the collected data, circuit elements displayed errors below 5%.

In general, the electrical properties at the working electrode surface were monitored by CV, EIS, and SWV studies using a redox probe solution of 5.0×10^{-3} mol/L $[Fe(CN)_6]^{3-}$ and 5.0×10^{-3} mol/L $[Fe(CN)_6]^{4-}$ in PBS buffer pH 7.4.

2.4. Preparation of C-SPE biosensor

The approach used to build the current biosensor is described in Fig. 1 and was inspired by our previous work on malaria and Zika diagnostics [29,30]. The first step involves the dispersion of carboxylated SWCNT in DMF (1.0 mg/mL) during 60 min. Then, the working electrode was incubated with 1.16 μL of the SWCNT solution and dried at 72 °C for 30 min (Fig. 1A). In the next step, the carboxyl groups on the surface of SWCNT were activated with a solution of EDAC and NHS (0.025 mol/L EDAC and 0.0125 mol/L NHS) for 90 min in a humid chamber at room temperature. The *p*-phenylenediamine (0.02 mol/L) was then bound to the SWCNT by incubation for 60 min to obtain an amine layer on the working electrode (Fig. 1B). Finally, S protein (0.019 mg/mL) was bound to the amine layer for 40 min at room temperature and in a humid environment (Fig. 1C). All solutions were prepared in PBS buffer pH 7.4, unless otherwise indicated. Subsequently, the analytical performance of the biosensor was determined by detecting antibodies bound to the S protein (Fig. 1D).

2.5. Characterization by Raman spectroscopy

Each step of the sensor design was followed by Raman spectroscopy by direct analysis of the material in a Thermo Scientific DXR Raman spectroscope equipped with a 532 nm laser. The average signal-to-noise ratio (peak height/RMS noise) was allowed for 900 s of measurement time, after up to 2 min of photobleaching, with up to 3 mW of laser power and a 50 μm slit aperture.

2.6. Ethics statement

Human serum was collected at Centro Hospitalar e Universitário de Coimbra (CHUC) from patients with or without a clinical history of COVID -19 and without concomitant comorbidities (cardiovascular, autoimmune, or respiratory disease). Positive samples were collected randomly during routine blood analysis by the clinicopathology service of the University Hospital of Coimbra (Patients details is shown in Table S1). The collected human samples were immediately frozen until use. This study was approved by the CHUC Ethics Committee (Process number OBS.SF.220-2021), always ensuring the protection of personal data through anonymization (General Data Protection Regulation 2016/679).

2.7. Analytical performance of the biosensor

The analytical performance of the sensor layer was evaluated by incubation with increasing standard concentrations of antibody solutions (anti-S protein) ranging from 1 pg/mL to 10 ng/mL prepared in PBS buffer pH 7.4. Each standard was incubated for 40 min at room temperature in a humidified environment. After incubation with each standard concentration, the sensor was washed and its impedimetric properties were analysed by EIS using the iron redox probe. The analytical response of the biosensor was also evaluated in negative human serum, i.e., serum without anti-S protein antibodies, which served as a control and was spiked with known standard concentrations of anti-S protein antibodies. Standards were prepared in negative human serum diluted 500-fold in PBS buffer pH 7.4, and the incubation time was set at 40 min. All assays were performed in triplicate.

The limit of detection (LOD) corresponded to the $x + 3\sigma$, where x is the average value of the EIS blank signals (obtained in the absence of anti-S protein) and σ is the known standard deviation of the EIS blank signal in successive measurements [31].

Biosensor selectivity was evaluated by incubation with the anti-N protein antibody in the same concentration range used to determine the calibration curve with the anti-S protein antibody. Similarly, the incubation time was set at 40 min and all electrochemical assays were performed in triplicate.

2.8. Analysis of human serum samples by VIDAS®

Immunoassay tests were performed using the VIDAS® equipment

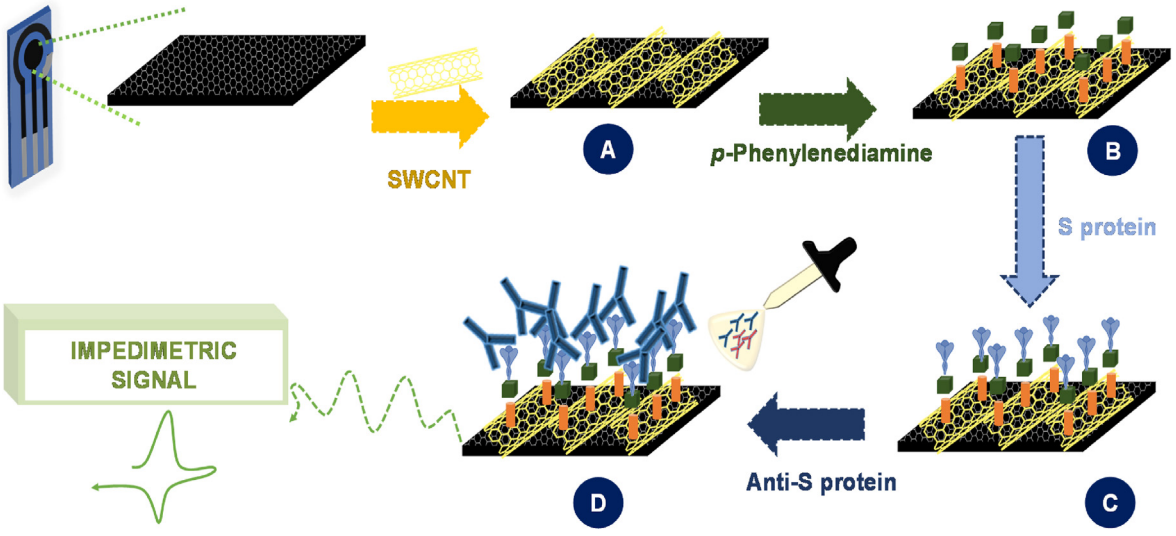

Fig. 1. Schematic representation of the C-SPEs and the functionalization of the working electrode: (A) addition of carboxylated SWCNT; (B) modification with *p*-phenylenediamine through EDAC/NHS coupling reaction; (C) binding of S protein and (D) electrochemical detection of anti-S protein antibody.

from Biomérieux (Marcy l'Etoile, France). This instrument performs an automated qualitative ELISA for the detection of specific anti-SARS-CoV-2 IgG in human serum, which requires the use of the VIDAS SARS -CoV-2 IgG 423834-02® kit (BioMérieux, Marcy l'Etoile, France). This kit contains the disposable solid phase strips, solid phase vials containing humanized recombinant SARS-CoV-2 antigen, the standard (with humanized recombinant anti-SARS-CoV-2 IgG antibody), and the positive (also with humanized recombinant anti-SARS-CoV-2 IgG antibody) and negative controls (without the humanized recombinant anti-SARS-CoV-2 IgG antibody) (https://www.biomerieux-diagnostics.com/vidas-sars-cov-2). In addition, the solutions used to generate the standard curve were obtained by successive dilutions of the purified anti-SARS-CoV-2 S-protein S1 recombinant antibody from BioLegend (San Diego, CA, USA).

The different solutions of the purified anti-SARS-CoV-2 S-protein S1 recombinant antibody were prepared. Then, 100 μL of these solutions were added to a designated spot on the kit strip and the automated qualitative ELISA was performed. First, the instrument dilutes the contents of the container. Then, the coated antigen captures the SARS-CoV-2 specific IgG, and a wash step follows to remove the unbound components. In a second step, the mouse monoclonal antibodies conjugated with alkaline phosphatase specifically recognize the IgG present in the contents. Again, the device performs a wash step to remove the unbound components. Finally, the instrument performs an incubation step by adding the substrate 4-methyl-umbelliferyl phosphate to the sample/standard, which is hydrolysed to the fluorescent product 4-methyl-umbelliferone. The fluorescence of this product is measured at 450 nm and a relative fluorescence value (RFV) is generated (Fig. S1) [32].

2.9. Correlation of VIDAS® signal with standard anti-S solutions

Even though VIDAS® gives an RFV value, the information it provides is only qualitative. It is considered a positive result if the test value (which is the quotient between the RFV of the sample and the RFV of the instrument standard 1) is equal to or above 1.00, and negative if it is below 1.00 [32,33] However, the RFV values are proportional to the concentration when anti-S standard solutions are analysed by VIDAS®. This allows the conversion of RFV values to concentration. To this end, anti-S standards of 0; 1.0; 5.0; 10.0; 25.0; 50.0; 100; 250 μg/mL were analysed by VIDAS®.

2.10. Analysis of human sera with the electrochemical biosensor

The positive serum samples were tested to evaluate the biosensor response compared to the VIDAS® results. The serum samples only had to be diluted beforehand (500-fold dilution in PBS, pH 7.4) to fit within the linear range of the sensitive biosensor and avoid interference from the serum matrix. All assays were performed in triplicate.

2.11. Synthesis of quantum dots and conjugation with anti-human IgG antibodies

Red emitting cadmium telluride quantum dots capped with 3-mercaptopropionic acid CdTe@MPA QDs were prepared according to a previous protocol with minor modifications [23]. Conjugation of antibodies with red emitting CdTe@MPA QDs was performed as follows. A solution of QDs (2.5 mg/mL) in PBS 0.01 mol/L pH 7.2 was incubated with goat anti-human IgG (51.02 μg/mL), EDAC (1.25 mg/mL), and NHS (1.50 mg/mL) for 3 h at room temperature in a total volume of 100 μL. Then, 30 mL of glycine (10 mmol/L) was added and the reaction mixture was incubated at room temperature for 30 min. Finally, the resulting solution was centrifuged at 8500 rpm for 3 min in the Amicon™ Ultra-0.5 centrifugal filter device. The filtrate solution was discarded, and the membrane was inverted to collect the anti-human IgG@QDs conjugates at the final concentration of 51.02 μg/mL. The procedure was repeated for the preparation of anti-human IgG@QDs at 10.10 μg/mL and 101.01 μg/mL (Fig. S2).

2.12. Secondary anti-human IgG@QDs as electrochemical labels

First, different concentrations of secondary goat anti-human IgG antibodies (10.10, 51.02, and 101.01 μg/mL) labelled with CdTe QDs were each incubated on one of the three sensor-modified surfaces with the maximum positive serum concentration detected by our biosensor (752 ng/mL) to select the optimal concentration for signal detection (Fig. S2). The composite working electrode surface of five other biosensors was incubated with PBS pH 7.4 for 40 min at room temperature until stabilized. Then, positive serum solutions diluted in negative serum (107, 150, 188, 250, and 752 ng/mL) were incubated on each of the five composite sensors. The selected concentration of QDs-labelled IgG antibody conjugates was then added to our device to label the primary antibodies present in the positive serum by incubating it at room temperature for 90 min. Instead of a redox probe, a solution containing 0.1 mol/L KCl as electrolyte was used to allow a more practical direct reading. The parameters of the SWV method had a potential range of −1.0 V to −0.2 V, with a potential step of 2.5 mV with an amplitude of 0.02 V at a frequency of 2 Hz.

3. Results and discussion

3.1. Biosensor assembly and characterization

The biosensor was constructed in three steps: Carboxylation of the carbon substrate, subsequent amination of this surface, and adsorption of S-protein. The preparation of an aminated surface directly on the carbon substrate could combine the first two steps and further simplify the procedure, but this was tried in several other ways that did not show sufficiently satisfactory results in terms of electrochemical stability to be a convincing electrochemical biosensor for global application.

The electrochemical features of the C-SPEs in each of these steps were followed by CV, EIS and SWV tests, with a standard iron redox probe, whose typical data are shown in Fig. 2. Carboxylation of the carbon working electrode on the C-SPEs was performed by casting carboxylated SWCNTs. As expected, the electrochemical properties showed that the electrical properties of the sensing layer were improved after modification with carboxylated carbon nanotubes. The effectiveness of this step was more evident in the EIS and SWV data, with a lower Rct value of ~549 Ω and a higher current of ~48.62 μA, respectively, compared to the original readings. After this modification, amination of the working electrode with *p*-phenylenediamine was achieved by an EDAC/NHS coupling reaction between the carboxyl groups of SWCNT and an amine group of *p*-phenylenediamine [34]. Subsequently, the S-protein was incubated on the amine layer, which resulted in a decrease in current at both CV (~83.68 μA) and SWV (~33.98 μA). In addition, a significant increase in Rct (1038.67 Ω) was observed. These results suggest that the S-protein recognition layer was successfully formed on the electrode.

The chemical modification of each step of the biosensor construction was followed by Raman spectroscopy (Fig. S3). The typical G and D bands of the C-SPE were located at 1583.0 cm^{-1} and 1350.8 cm^{-1}, respectively, indicating the presence of a graphitic nanomaterial with sp^2 and sp^3 carbon-hybridization systems. Incubation of the carboxylated SWCNT onto the working electrode significantly changed the Raman spectra obtained. The G and D bands were now at 1590.62 cm^{-1} and 1342.21 cm^{-1}, respectively, with the D band decreasing more than tenfold compared to the G band. Overall, this confirmed the presence of the carbon nanotubes on the C-SPE [35]. Subsequent addition of EDAC/NHS, *p*-phenylenediamine, S-protein, and anti-S-protein antibodies did not result in significant changes in Raman spectra, also confirmed by calculating the ratios of the intensities of G and D bands (Table S2). Overall, the significant change in Raman spectra was observed only after the

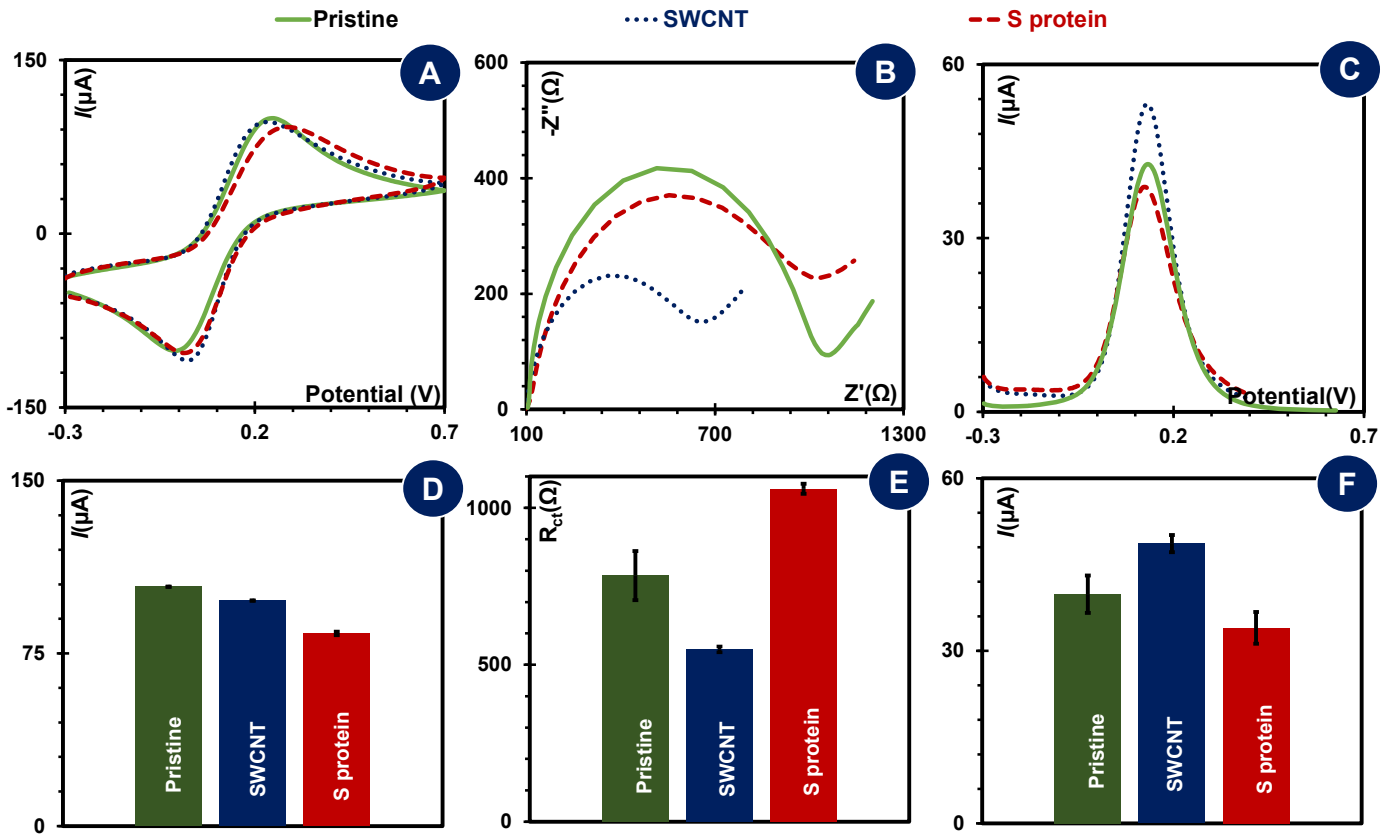

Fig. 2. Electrochemical data collected upon the biosensor construction, using CV (A), EIS (B) and SWV (C) measurements. Data includes pristine C-SPEs, after modified with SWCNT and S protein. Graphics D and F show the current peak's intensity, and graphic E presents the R_{ct} values with the respective error bars, highlighting the reproducibility of three independent devices.

incubation of the carboxylated SWCNTs, with only minor changes in the D-band and G-band observed in the subsequent phases of the biosensor assembly.

3.2. Analytical performance in PBS buffer

The analytical properties of the biosensor were evaluated by testing increasing concentrations of the anti-S protein antibody, followed by EIS measurements and the generation of calibration curves. The typical Nyquist plots of the EIS measurements are shown in Fig. 3A. They show a positive correlation between the increase in Rct and the successive increase in antibody concentration. These results indicate that the impedimetric resistance, i.e., the diameter of the semicircles in the Nyquist plots, increases with increasing amount of antibody that recognizes and binds the S protein. The sensor showed a linear range between 1.0 pg/mL and 10.0 ng/mL, while higher concentrations saturate the sensor layer (Fig. 3B). The reproducibility of the sensor system was confirmed by performing three independent calibrations, with new

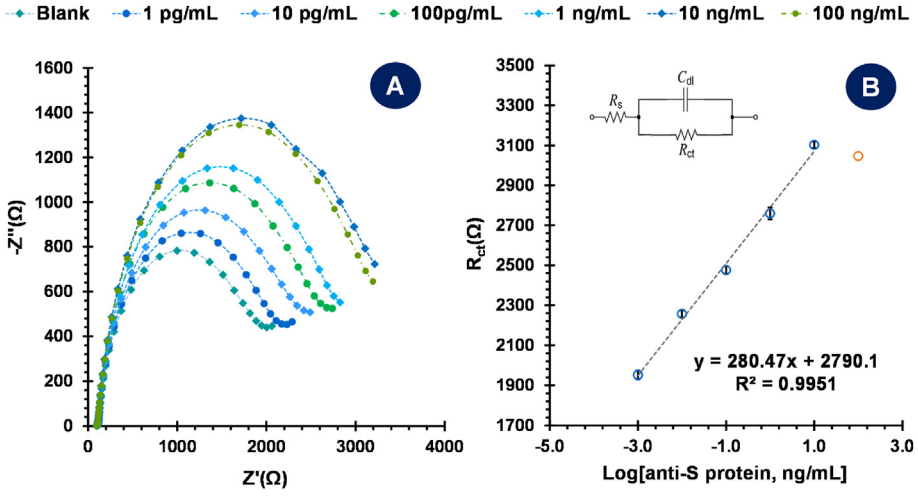

Fig. 3. EIS measurements of the calibration with anti-S protein antibodies (1.0 pg/mL – 100 ng/mL) in PBS buffer: Nyquist plots (A) and the corresponding calibration curve (B). Readings were performed with the redox pair 5.0×10^{-3} mol/L $[Fe(CN)_6]^{3-}$ and 5.0×10^{-3} mol/L $[Fe(CN)_6]^{4-}$ prepared in 0.01 mol/L PBS buffer pH 7.4.

biosensing units. The relative standard deviation of the slope was ~2.6%, with an average slope of 280.47 Ω/decade. The squared correlation coefficient of the calibrations was >0.99. The reproducibility of the electrochemical response was excellent, proving that the system is reproducible, considering that the RSD values ranged from 0.5% (minimum) to 1.11% (maximum) in a linear trend. Overall, these results showed a highly sensitive response to anti-S protein antibodies with a LOD of 0.77 pg/mL.

3.3. Selectivity of the biosensor

The biosensor had a recombinant S protein on the surface of the working electrode so that it should bind selectively to anti-S protein antibodies. This selective binding may be confirmed by examining the response of the biosensor to other competing compounds. Since infected humans also have anti-N protein antibodies, it was considered here to evaluate the selectivity by checking the cross-reactivity of the biosensor with these specific antibodies. Distinguishing between antibodies to S and N proteins is also critical for tracking COVID -19. Technically, anti-N proteins are expected to interfere little to not at all with the measurement of anti-S proteins.

In this study, the selectivity of the biosensor was evaluated by examining the response to individual solutions of anti-N and anti-S protein antibodies prepared in the same concentration range over the concentration range of the linear response. The data collected considered the Rct values obtained in each EIS measurement, and the average values were plotted in Fig. 4. In general, in the presence of the anti-N protein antibody, the biosensor showed a uniform response (like the blank) over the entire concentration range tested. This contrasted with the increasing Rct values of the biosensor in the presence of the increasing concentrations of anti-S protein antibody.

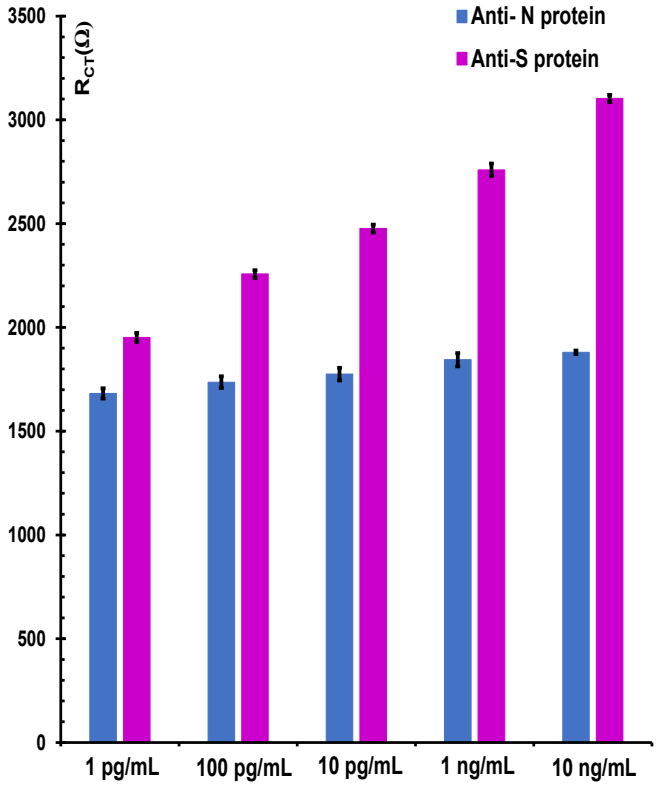

Fig. 4. EIS response of the biosensor in the form of Rct values after the incubation of anti-S or anti-N protein antibodies, ranging from 1.0 pg/mL to 10 ng/mL.

Overall, the data suggest that the current biosensor is not affected by the presence of the anti-N protein antibody and that it responds accurately to the anti-S protein antibody. These are interesting results, as any analytical tool capable of distinguishing spike-from nucleocapsid-specific immunity can help to study the immunological response of post-infected or vaccinated individuals [10,36].

3.4. Analytical performance in spiked human serum

The analytical performance of the sensing layer was evaluated using negative human serum spiked with anti-S protein antibodies to provide more realistic information in the context of real-world applications. The negative serum was diluted 500-fold to better match the sample to the linear trend of the biosensor. The EIS measurements were used to evaluate the biosensor response, and the calibration curves were plotted as Rct versus the logarithm of concentration (Fig. 5). Rct values increased with increasing antibody concentration (Fig. 5A), and a linear trend was confirmed in the range of 1.0 pg/mL and 10 ng/mL. The average slope was 1825.5 Ω/decade, which was greater than that of the buffer, indicating that sensitivity increased. This likely reflects the higher complexity of the sample matrix (including higher ion and protein content), as the absolute Rct values were higher than those of the buffer at comparable concentrations. Overall, the biosensor provided reproducible responses, with relative standard deviations of slope of ~4.0. The squared correlation coefficient of all calibrations was also >0.99, confirming the quality of the linear trend (Fig. 5B). Overall, these results showed a sensitive response to detect anti-S antibodies with a very low LOD. Although tested in a more complex matrix, LOD was not significantly different from LOD in PBS buffer pH 7.4 and was 0.70 pg/mL. This LOD is in the range or even lower than recent findings reported in the literature for other electrochemical biosensors, mostly also containing nanomaterials that improve the sensitivity (Table S3).

Considering the detection of antibodies in infected humans and because the serum was diluted 500-fold, the biosensor can be used to analyse human sera from 0.5 ng/mL to 5000 ng/mL. This is a wide concentration range that will simplify future application procedures, although more concentrated solutions may saturate the biosensor and require additional dilution. However, further testing was performed with positive samples, as the level in the serum of a healthy person (negative serum) is quite different from that of a person with COVID -19.

3.5. Analysis of positive sera samples

The ability of the electrochemical biosensor to determine antibody levels in different positive human samples was tested by analyzing the same samples with both the biosensor and VIDAS®. Since VIDAS® only provides qualitative data (positive or negative) in terms of antibody levels in sera, we generated a standard curve using different standard solutions of purified anti-SARS-CoV-2 S1 recombinant protein antibodies. The RFV values obtained for these antibodies (expressed in arbitrary units) were correlated with the logarithm of the antibody concentration, enabling the extraction of quantitative data from this commercial method. The data obtained are shown in Fig. S4 and consider only the concentration range of the antibodies, which have a linear behaviour. The anti-S-SARS CoV-2 IgG concentration in the sera could be now calculated by intersecting this curve, which gives an idea of the range of anti-S protein IgG antibody concentrations in the COVID-19 positive population.

The samples included in this comparative study contained different ranges of antibody concentrations (n = 5), as expected given the quite variable RFV concentrations in VIDAS®. The concentrations chosen for this purpose are well above the capabilities of the biosensor and range from 5 to 230 μg/mL. Prior to analysis, samples were treated according to the method used. For VIDAS®, the procedure provided by the commercial instrument was used, while for the biosensor only an appropriate dilution was performed.

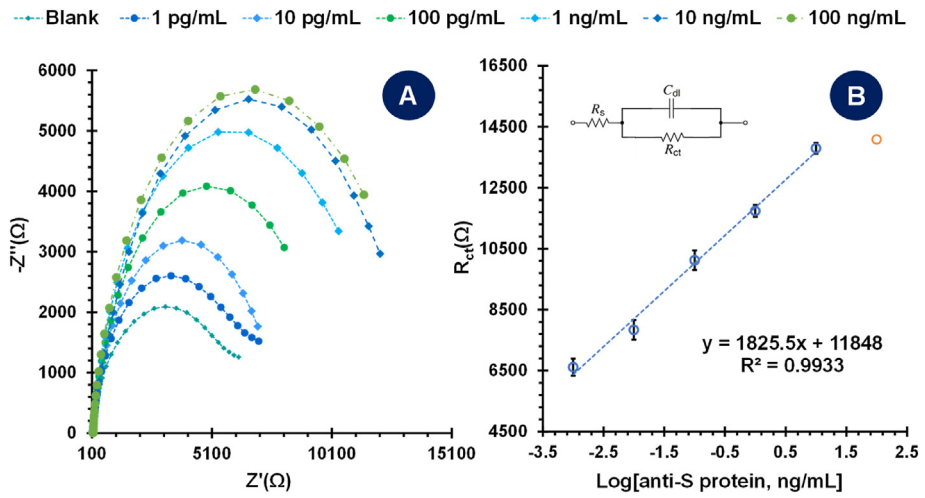

Fig. 5. EIS measurements of the calibration with anti-S protein antibodies (1.0 pg/mL – 100 ng/mL) spiked in negative human serum (500-fold diluted in PBS buffer): Nyquist plots (A) and the corresponding calibration curve (B). Readings were performed with the redox pair 5.0×10^{-3} mol/L $[Fe(CN)_6]^{3-}$ and 5.0×10^{-3} mol/L $[Fe(CN)_6]^{4-}$ prepared in 0.01 mol/L PBS buffer pH 7.4.

The concentrations of these samples obtained with VIDAS® and the biosensor are shown in Table S4. The concentrations obtained with the biosensor were extracted from the correlation of the log concentration of antibodies known to be present in the samples with the Rct values of each of these positive samples (Fig. S5). This was done to provide a valuable correlation between the positive sera and the electrochemical method, which proved necessary to eliminate the effect of the sample matrix now containing additional biomolecules required to combat the disease. Attempts were made to compare the readings with the concentrations of antibodies diluted in negative sera, but the data obtained were not reliable. It was also noted that the Rct values increased well beyond the usual calibration ranges, which indeed confirmed some influence of the positive samples, but these had no significant effect upon the concentration of antibodies yielding a linear trend.

Overall, the relative errors in this analysis ranged from −10.2 to +15.3%. Considering that these are human samples, these results can be considered accurate [37,38]. Furthermore, these are excellent results considering that the samples were highly diluted in the biosensor measurements and that the two methods have very different operating principles. This also indicates that the biosensor can be considered an important alternative to current methods, especially when lower amounts of antibodies are involved.

3.6. Comparison of method capabilities to low antibody concentrations

From the data obtained, it appeared that the biosensor was able to detect much lower concentrations of antibodies than VIDAS®. To confirm this, a positive human sample with a concentration of approximately 225.66 μg/mL was diluted down to different concentration levels and evaluated using both methods.

VIDAS® was only able to measure concentrations up to 2256 ng/mL, which corresponds to a 100-fold dilution of the original sample. At higher serum dilutions, corresponding to 150, 107, and 83 ng/mL, the analytical signal in VIDAS® was similar, indicating that the concentration was equal to or lower than 2.3 μg/mL and that further concentration differences could not be distinguished. Overall, VIDAS® was unable to discriminate between antibody concentrations below 2.3 μg/mL. This is a fairly high concentration and confirms the limited ability of the comparative method to provide accurate data for lower antibody concentrations (the commercial method works well but only provides reliable data for higher concentrations).

In contrast, serial dilution of this sample resulted in a linear trend against antibody concentration by EIS. This was achieved when the concentration incubated on the biosensor ranged from 70 to 752 ng/mL, with clearly distinguishable values for concentrations of 150, 107, and 83 ng/mL. The electrochemical biosensor was thus able to detect differences between samples that had much lower concentrations than those analysed by VIDAS®, down to 70 ng/mL. Validation of the data obtained by EIS was not performed because we were not aware of any method suitable for comparison at such low concentrations. This unique feature of the proposed devices could be a valuable tool for future epidemiological studies and for understanding changes in antibody levels associated with vaccination (as a recommendation for clinicians on when to recommend a new vaccine dose).

3.7. Alternative electrochemical analysis of human sera

Considering the good results obtained in testing positive human serum with the electrochemical biosensor, another proof-of-concept was explored by developing and using nanoparticles as electrochemical markers bound to secondary antibodies. These secondary antibodies bind the anti-S protein antibodies recognised on the surface of the biosensor and generate an electrochemical signal. For this purpose, the secondary antibodies were labelled with CdTe QDs, which are nanoscale colloidal semiconductor crystals that have electrochemical properties (Fig. S2) [24]. The electrochemical results of the QDs were investigated in terms of metal oxidation by SWV, moving from −1.0 V to positive potentials.

In a proof-of-concept study, different concentrations of anti-human IgG antibodies labelled with CdTe-QDs were tested to evaluate their effects on current measurements at the sensor surface (Fig. 6). The most diluted and the most concentrated solutions of the IgG antibodies produced similar current values (1.60 μA and 1.63 μA, respectively). Therefore, considering the fluorescence values obtained for the different concentrations of QDs-labelled IgG antibodies, we decided to label the primary antibodies with the lower concentration of IgG antibodies (10.10 μg/mL), as this could be a more dispersed solution containing a higher ratio of CdTe-QDs nanocrystals for each IgG antibody (thereby amplifying the signal).

In this approach, the biosensor was first incubated in a solution containing diluted positive serum (107, 150, 188, 250, or 752 ng/mL) and then in a solution containing anti-human IgG@QDs of 10.10 μg/mL. The SWV data obtained for these concentrations are shown in Fig. 6D and reflect the metal oxidation readings. The current signals decreased with increasing antibody concentration, yielding a linear trend when the peak height values were plotted against the log concentration of the antibody (150 ng/mL to 752 ng/mL). In principle, one would expect that a higher

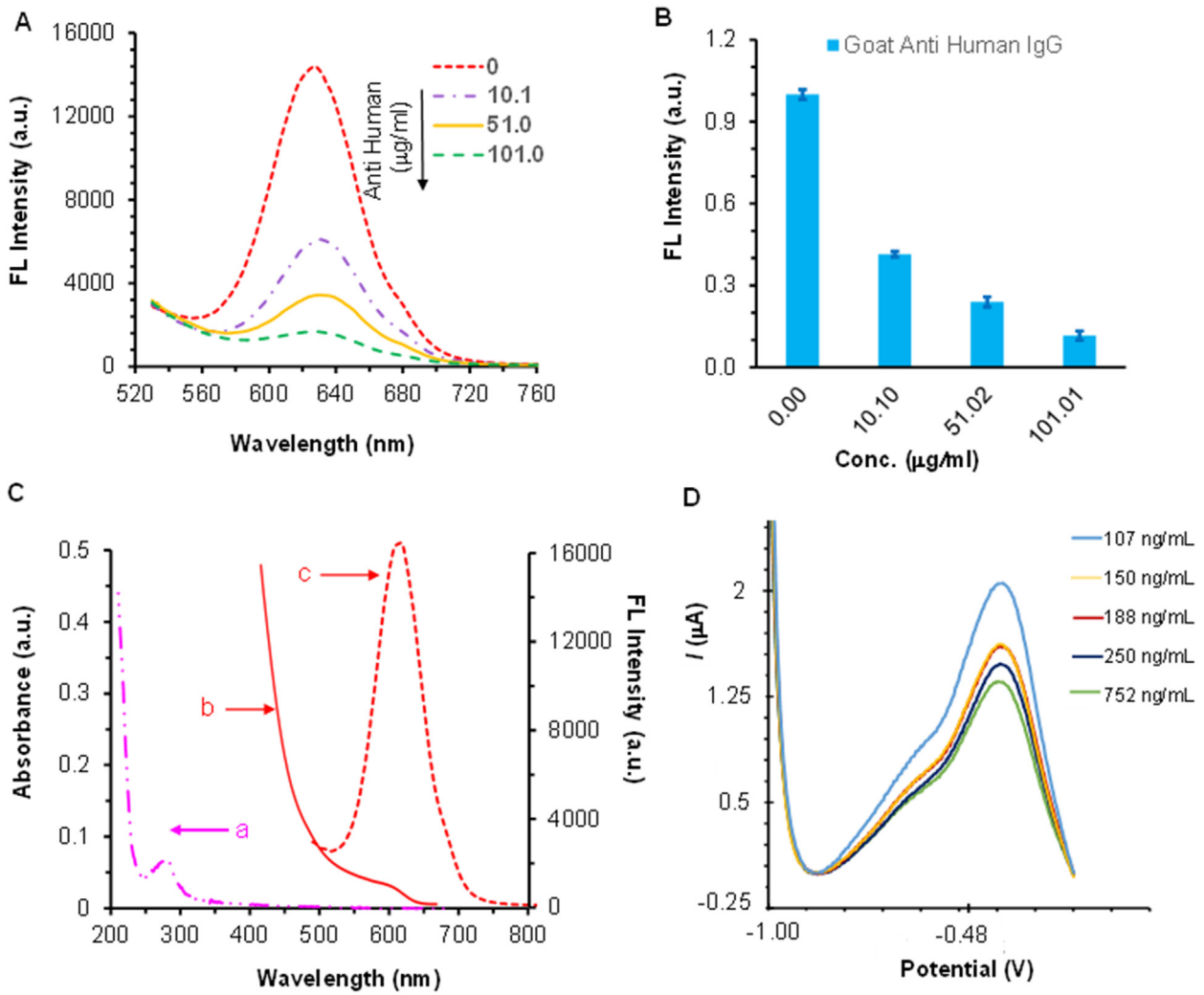

Fig. 6. (A and B) Fluorescence signals of red emitting QDs in the presence of increasing concentrations of goat anti-human IgG, in PBS 0.01 mol/L pH 7.2. (C) UV–vis absorption spectra of goat anti-human IgG in PBS 0.01 mol/L pH 7.2 (a) and the UV/vis spectra of red emitting QDs 2.5 mg/mL in PBS 0.01 mol/L pH 7.2, (b) along with the correspondent fluorescent spectra (c). (D) SWV voltammograms of different concentrations of positive serum containing primary antibodies conjugated with a 10.10 ng/mL concentration of IgG secondary antibodies labelled with CdTe QDs.

amount of anti-S antibody would lead to a higher number of IgG@QDs conjugates, which in turn should lead to a higher current value due to the higher amount of QDs. However, the system may undergo opposite effects during the incubation of the IgG@QDs conjugates. While the antibodies block the electrical surface and decrease the current signals, the current value of the observed peak increases with increasing number of QDs. Since this leads to opposite effects and the linear trend has a negative slope, it was obvious that the anti-IgG dominated the signal obtained.

In any case, this proof-of-concept approach is an alternative way to read the electrochemical response if one wishes to obtain a more selective response. Alternatively, direct electrochemical measurements using the iron redox probe already outperform conventional methods such as VIDAS® in terms of LOD and sensitivity.

4. Conclusions

A rapid serological test to diagnose and/or monitor immunity after SARS-CoV-2 infection or vaccination remains a challenge given current technologies. ELISA-based methods are not very sensitive and reliable quantitative information is scarce. Here we demonstrate the successful development of a simple, innovative, highly sensitive and selective biosensor for the detection of antibodies to the S protein in human serum. This novel electrochemical biosensor can be used post-infection or post-vaccination when circulating antibody concentrations are lower and cannot be detected by conventional ELISA methods. Its detection capabilities significantly outperform commercial methods available on the market and are comparable or better than other electrochemical methods described in the literature.

It is important to note that a cross-response of the biosensor against other SARS virus was not evaluated. However, a cross-reactivity with other antibodies against these means that one's serum has antibodies that also recognize S protein, meaning that there is an expected degree of protective immunity conferred by these. Thus, as the main target of the biosensor is to monitor the protective immunity by means of antibodies, an eventual cross-reactivity would not hamper the result of a test provided by this biosensor in point-of-care.

Overall, the biosensor provides very low LOD values and can reach very low concentrations of positive sera when testing human sera. Therefore, the biosensor described here has the potential to become a valuable tool for early diagnosis and monitoring of antibody levels during vaccination follow-up. Future work will therefore focus on miniaturization and the use of different nanomaterials as well as an environmentally friendly substrate, as paper. The development of multiplex biosensors covering a variety of different viruses is also foreseeable.

Author statement

Ana R. Cardoso. Investigation. Methodology. Formal analysis. Validation. Visualization. Data Curation. Writing - original draft. *João Frederico Alves.* Investigation. Formal analysis. Validation. Writing - original draft. *Manuela F. Frasco.* Investigation. Methodology. Formal analysis. Validation. Writing - review & editing. *Ana Margarida Piloto.* Investigation. Formal analysis. Validation. Writing - original draft. *Verónica Serrano.* Investigation. Formal analysis. *Daniela Mateus.* Investigation. Methodology. Formal analysis. *Ana Isabel Sebastião.* Investigation. Methodology. Formal analysis. *Ana Miguel Matos.* Validation. Resources. Formal analysis. Supervision. *Anália do Carmo.* Validation. Data curation. Writing - review & editing. *Teresa Rosete.* Methodology. Validation. Resources. Project administration. Supervision. *Elvira Fortunato.* Resources. Writing - review & editing. Supervision. *M. Goreti F. Sales.* Conceptualization. Methodology. Funding acquisition. Project administration. Supervision. Visualization. Writing - review & editing.

Declaration of competing interest

The authors declare that they have no known competing financial interests or personal relationships that could have appeared to influence the work reported in this paper.

Acknowledgements

The authors acknowledge funding through project TecniCov (POCI-01-02B7-FEDER-069745), co-funded by FEDER through COMPETE2020 and Lisboa2020 and CY-Sensors (POCI-01-0145-FEDER-032359) through Fundação para a Ciência e a Tecnologia (FCT), Portugal. ARC acknowledge funding to National Foundation for Science and Technology, I.P., Portugal (FCT) through the PhD. Grant, reference SFRH/BD/130107/2017.

Appendix A. Supplementary data

Supplementary data to this article can be found online at https://doi.org/10.1016/j.mtbio.2022.100354.

References

[1] WHO, Managing epidemics, Thomson Pr, Switzerland, 2018.
[2] A.G.P. Ross, S.M. Crow, M.W. Tyndal, Planning for the next global pandemic, Int. J. Infect. Dis. 38 (2015) 89–94, https://doi.org/10.1016/j.ijid.2015.07.016.
[3] P. Zhou, X. Lou Yang, X.G. Wang, B. Hu, L. Zhang, W. Zhang, H.R. Si, Y. Zhu, B. Li, C.L. Huang, H.D. Chen, J. Chen, Y. Luo, H. Guo, R. Di Jiang, M.Q. Liu, Y. Chen, X.R. Shen, X. Wang, X.S. Zheng, K. Zhao, Q.J. Chen, F. Deng, L.L. Liu, B. Yan, F.X. Zhan, Y.Y. Wang, G.F. Xiao, Z.L. Shi, A pneumonia outbreak associated with a new coronavirus of probable bat origin, Nature 579 (2020) 270–273, https://doi.org/10.1038/s41586-020-2012-7.
[4] D.K.W. Chu, Y. Pan, S.M.S. Cheng, K.P.Y. Hui, P. Krishnan, Y. Liu, D.Y.M. Ng, C.K.C. Wan, P. Yang, Q. Wang, M. Peiris, L.L.M. Poon, Molecular diagnosis of a novel coronavirus (2019-nCoV) causing an outbreak of pneumonia, Clin. Chem. 66 (2020) 549–555, https://doi.org/10.1093/clinchem/hvaa029.
[5] H. Nishiura, T. Kobayashi, T. Miyama, A. Suzuki, S. Jung, K. Hayashi, R. Kinoshita, Y. Yang, B. Yuan, A.R. Akhmetzhanov, N.M. Linton, Estimation of the asymptomatic ratio of novel coronavirus infections (COVID-19), Int. J. Infect. Dis. 94 (2020) 154–155, https://doi.org/10.1016/j.ijid.2020.03.020.
[6] B. Sun, Y. Feng, X. Mo, P. Zheng, Q. Wang, P. Peng, X. Liu, Z. Chen, H. Huang, F. Zhang, W. Luo, X. Niu, P. Hu, L. Wang, H. Peng, L. Feng, F. Li, F. Zhang, F. Li, N. Zhong, L. Chen, Kinetics of SARS-CoV-2 specific IgM and IgG responses in COVID-19 patients, Emerg. Microb. Infect. 9 (2020) 940–948, https://doi.org/10.1080/22221751.2020.1762515.
[7] K.K.-W. To, O.T.-Y. Tsang, W.-S. Leung, A.R. Tam, T.-C. Wu, D.C. Lung, C.C.-Y. Yip, J.-P. Cai, J.M.-C. Chan, T.S.-H. Chik, D.P.-L. Lau, C.Y.-C. Cho, L.-L. Chen, W.-M. Chan, K.-H. Chan, J.D. Ip, A.C.-K. Ng, R.W.-S. Poon, C.-T. Luo, V.C.-C. Cheng, J.F.-W. Chan, I.F.-N. Hung, Z. Chen, H. Chen, K.-Y. Yuen, Temporal profiles of viral load in posterior oropharyngeal saliva samples and serum antibody responses during infection by SARS-CoV-2 : an observational cohort study, Lancet Infect. Dis. 20 (2020) 565–574, https://doi.org/10.1016/S1473-3099(20)30196-1.
[8] J.D. Whitman, J. Hiatt, C.T. Mowery, B.R. Shy, R. Yu, T.N. Yamamoto, U. Rathore, G.M. Goldgof, C. Whitty, J.M. Woo, A.E. Gallman, T.E. Miller, A.G. Levine, D.N. Nguyen, S.P. Bapat, J. Balcerek, S.A. Bylsma, A.M. Lyons, S. Li, A.W. Wong, E.M. Gillis-buck, Z.B. Steinhart, Y. Lee, R. Apathy, M.J. Lipke, J.A. Smith, T. Zheng, I.C. Boothby, E. Isaza, J. Chan, D.D.A. Ii, J. Lee, T.A. Macrae, T.S. Kyaw, D. Wu, D.L. Ng, W. Gu, V.A. York, H.A. Eskandarian, L.A. Farrington, R.P. Loudermilk, K. Koshal, K.C. Zorn, W.F. Garcia-beltran, D. Yang, M.G. Astudillo, B.E. Bernstein, J.A. Gelfand, E.T. Ryan, R.C. Charles, A.J. Iafrate, J.K. Lennerz, S. Miller, C.Y. Chiu, S.L. Stramer, M.R. Wilson, J.G. Cyster, J.D. Ernst, A.H.B. Wu, K.L. Lynch, C. Bern, P.D. Hsu, A. Marson, Evaluation of SARS-CoV-2 serology assays reveals a range of test performance, Nat. Biotechnol. 38 (2020) 1174–1183, https://doi.org/10.1038/s41587-020-0659-0.
[9] M.A. Macmullan, A. Ibrayeva, K. Trettner, L. Deming, S. Das, F. Tran, J.R. Moreno, J.G. Casian, P. Chellamuthu, J. Kraft, K. Kozak, F.E. Turner, V.I. Slepnev, L.M. Le Page, ELISA detection of SARS - CoV - 2 antibodies in saliva, Sci. Rep. 10 (2020) 1–8, https://doi.org/10.1038/s41598-020-77555-4.
[10] N. Koerber, A. Priller, S. Yazici, T. Bauer, C. Cheng, H. Mijo, H. Wintersteller, S. Jeske, E. Vogel, M. Feuerherd, K. Tinnefeld, C. Winter, J. Ruland, M. Gerhard, B. Haller, C. Christa, O. Zelger, H. Roggendorf, M. Halle, J. Erber, P. Lingor, Dynamics of spike-and nucleocapsid speci fi c immunity during long-term follow-up and vaccination of SARS-CoV-2 convalescents, Nat. Commun. 13 (2022) 1–14, https://doi.org/10.1038/s41467-021-27649-y.
[11] N. Kumar, N.P. Shetti, S. Jagannath, T.M. Aminabhavi, Electrochemical sensors for the detection of SARS-CoV-2 virus, Chem. Eng. J. 430 (2022) 1–15, https://doi.org/10.1016/j.cej.2021.132966.
[12] A. Yakoh, U. Pimpitak, S. Rengpipat, N. Hirankarn, O. Chailapakul, S. Chaiyo, Paper-based electrochemical biosensor for diagnosing COVID-19 : detection of SARS-CoV-2 antibodies and antigen, Biosens. Bioelectron 176 (2021) 1–8, https://doi.org/10.1016/j.bios.2020.112912.
[13] S.K. Elledge, X.X. Zhou, J.R. Byrnes, A.J. Martinko, I. Lui, K. Pance, S.A. Lim, J.E. Glasgow, A.A. Glasgow, K. Turcios, N.S. Iyer, L. Torres, M.J. Peluso, T.J. Henrich, T.T. Wang, C.M. Tato, K.K. Leung, B. Greenhouse, J.A. Wells, Engineering luminescent biosensors for point-of-care SARS-CoV-2 antibody detection, Nat. Biotechnol. 39 (2021) 928–935, https://doi.org/10.1038/s41587-021-00878-8.
[14] O. Calvo-lozano, M. Sierra, M. Soler, M. Estévez, L. Chiscano-Cámon, A. Ruiz-Sanmartin, J.C. Ruiz-Rodriguez, R. Ferrer, J.J. González-López, J. Esperalba, C. Fernández-Naval, L. Bueno, R. López-Aladid, A. Torres, L. Fernández-Barat, S. Attoumani, R. Charrel, B. Coutard, L.M. Lechuga, Label-free plasmonic biosensor for rapid , quantitative , and highly sensitive COVID-19 serology : implementation and clinical validation, Anal. Chem. 94 (2022) 975–984, https://doi.org/10.1021/acs.analchem.1c03850. In press.
[15] A. Ali, C. Hu, S. Jahan, B. Yuan, M.S. Saleh, E. Ju, S. Gao, R. Panat, Sensing of COVID-19 antibodies in seconds via aerosol jet nanoprinted reduced-graphene-oxide-coated 3D electrodes, Adv. Mater. 33 (2021) 1–15, https://doi.org/10.1002/adma.202006647.
[16] X. Bin, E.H. Sargent, S.O. Kelley, Nanostructuring of sensors determines the efficiency of biomolecular capture, Anal. Chem. 82 (2010) 5928–5931, https://doi.org/10.1021/ac101164n.
[17] L. Soleymani, Z. Fang, E.H. Sargent, S.O. Kelley, Programming the detection limits of biosensors through controlled nanostructuring, Nat. Nanotechnol. 4 (2009) 844–848, https://doi.org/10.1038/nnano.2009.276.
[18] Z. Wang, Z. Dai, Carbon nanomaterial-based electrochemical biosensors: an overview, Nanoscale 7 (2015) 6420–6431, https://doi.org/10.1039/c5nr00585j.
[19] M. Pagán, D. Suazo, N. del Toro, K. Griebenow, A comparative study of different protein immobilization methods for the construction of an efficient nano-structured lactate oxidase-SWCNT-biosensor, Biosens. Bioelectron. 64 (2015) 138–146, https://doi.org/10.1016/j.bios.2014.08.072.
[20] N. Etminan, M. Yoosefian, H. Raissi, M. Hakimi, Solvent effects on the stability and the electronic properties of histidine/Pd-doped single-walled carbon nanotube biosensor, J. Mol. Liq. 214 (2016) 313–318, https://doi.org/10.1016/j.molliq.2015.12.009.
[21] H. Ashiba, Y. Sugiyama, X. Wang, H. Shirato, K. Higo-Moriguchi, K. Taniguchi, Y. Ohki, M. Fujimaki, Detection of norovirus virus-like particles using a surface plasmon resonance-assisted fluoroimmunosensor optimized for quantum dot fluorescent labels, Biosens. Bioelectron. 93 (2017) 260–266, https://doi.org/10.1016/j.bios.2016.08.099.
[22] Z. Deng, Y. Zhang, J. Yue, F. Tang, Q. Wei, Green and orange CdTe quantum dots as effective pH-sensitive fluorescent probes for dual simultaneous and independent detection of viruses, J. Phys. Chem. B 111 (2007) 12024–12031, https://doi.org/10.1021/jp074609z.
[23] A.M. Piloto, D.S.M. Ribeiro, S.S.M. Rodrigues, C. Santos, J.L.M. Santos, M.G.F. Sales, Plastic antibodies tailored on quantum dots for an optical detection of myoglobin down to the femtomolar range, Sci. Rep. 8 (2018) 1–11, https://doi.org/10.1038/s41598-018-23271-z.
[24] Q. Liu, X. Lu, J. Li, X. Yao, J. Li, Direct electrochemistry of glucose oxidase and electrochemical biosensing of glucose on quantum dots/carbon nanotubes electrodes, Biosens. Bioelectron. 22 (2007) 3203–3209, https://doi.org/10.1016/j.bios.2007.02.013.
[25] M.A. Macdonald, H.A. Andreas, Method for equivalent circuit determination for electrochemical impedance spectroscopy data of protein adsorption on solid surfaces, Electrochim. Acta 129 (2014) 290–299, https://doi.org/10.1016/j.electacta.2014.02.046.
[26] E.B. Bahadir, M.K. Sezgintürk, A review on impedimetric biosensors, Artif. Cells Nanomed. Biotechnol. 44 (2016) 248–262, https://doi.org/10.3109/21691401.2014.942456.
[27] F. Lisdat, D. Schäfer, The use of electrochemical impedance spectroscopy for biosensing, Anal. Bioanal. Chem. 391 (2008) 1555–1567, https://doi.org/10.1007/s00216-008-1970-7.

[28] N.O. Laschuk, E.B. Easton, O.V. Zenkina, Reducing the resistance for the use of electrochemical impedance spectroscopy analysis in materials chemistry, RSC Adv. 11 (2021) 27925–27936, https://doi.org/10.1039/d1ra03785d.
[29] G. Cabral-miranda, A.R. Cardoso, L.C.S. Ferreira, M.G.F. Sales, M.F. Bachmann, Biosensor-based selective detection of Zika virus speci fi c antibodies in infected individuals, Biosens. Bioelectron 113 (2018) 101–107, https://doi.org/10.1016/j.bios.2018.04.058.
[30] A.R. Cardoso, G. Cabral-miranda, A. Reyes-sandoval, M.F. Bachmann, M.G.F. Sales, Detecting circulating antibodies by controlled surface modi fi cation with speci fi c target proteins : application to malaria, Biosens. Bioelectron. 91 (2017) 833–841, https://doi.org/10.1016/j.bios.2017.01.031.
[31] D. Harvey, in: K. Kane (Ed.), Modern Analytic Chemistry, first ed.Mod. Anal. Chem., McGraw-Hill Higher Education, 2000, p. 797.
[32] N. Renard, S. Daniel, N. Cayet, M. Pecquet, F. Raymond, S. Pons, J. Lupo, C. Tourneur, C. Pretis, G. Gerez, P. Blasco, M. Combe, I. Canova, M. Lesénéchal, F. Berthier, Performance characteristics of the vidas SARS-CoV-2 IgM and IgG serological assays, J. Clin. Microbiol. 59 (2021) 1–14.
[33] M. Bubonja-Šonje, L. Batičić, M. Abram, Đ.C. Grbėsa, Diagnostic accuracy of three SARS-CoV2 antibody detection assays , neutralizing effect and longevity of serum antibodies, J. Virol. Methods 293 (2021) 1–7, https://doi.org/10.1016/j.jviromet.2021.114173.
[34] K. Jiang, L.S. Schadler, R.W. Siegel, X. Zhang, M. Terrones, Protein immobilization on carbon nanotubes via a two-step process of diimide-activated amidation, J. Mater. Chem. 14 (2004) 37–39.
[35] A.I. López-Lorente, B.M. Simonet, M. Valcárcel, Raman spectroscopic characterization of single walled carbon nanotubes : in fl uence of the sample aggregation state, Analyst 139 (2014) 290–298, https://doi.org/10.1039/c3an00642e.
[36] J.S. Terry, L. Br, M.S. Scherman, C.E. Mcalister, R. Perera, T. Schountz, B.J. Geiss, Development of a SARS-CoV-2 nucleocapsid specific monoclonal antibody, Virology 558 (2021) 28–37, https://doi.org/10.1016/j.virol.2021.01.003.
[37] D. Brinati, A. Campagner, D. Ferrari, M. Locatelli, G. Banfi, F. Cabitza, Detection of COVID-19 infection from routine blood exams with machine learning: a feasibility study, J. Med. Syst. 44 (2020) 1–12, https://doi.org/10.1007/s10916-020-01597-4.
[38] M. Plebani, Errors in clinical laboratories or errors in laboratory medicine? Clin. Chem. Lab. Med. 44 (2006) 750–759, https://doi.org/10.1515/CCLM.2006.123.